Video-rate wide-field coherent anti-Stokes Raman scattering microscopy with collinear nonphase-matching illumination

Ming Lei,[a,b] Martin Winterhalder,[a] Romedi Selm,[a] and Andreas Zumbusch[a]
[a]University of Konstanz, Department of Chemistry, D-78457 Konstanz, Germany
[b]Chinese Academy of Sciences, Xi'an Institute of Optics and Precision Mechanics, State Key Laboratory of Transient Optics and Photonics, Xi'an 710119, China

Abstract. A simple scheme for video-rate wide-field coherent anti-Stokes Raman scattering (CARS) microscopy is presented. The method is based on collinear nonphase-matching illumination. The mechanisms leading to CARS signal generation are investigated. We find that refraction-mediated phase-matching is the main effect. Video-rate wide-field CARS microscopy of polystyrene beads and CARS wide-field images of *C. elegans* embryos are shown, and the capabilities and the limitations of the scheme are discussed. © *2011 Society of Photo-Optical Instrumentation Engineers (SPIE)*. [DOI: 10.1117/1.3533707]

Keywords: coherent anti-Stokes Raman scattering microscopy; wide field; video-rate.

Paper 10297SSR received Jun. 3, 2010; revised manuscript received Jun. 25, 2010; accepted for publication Jun. 28, 2010; published online Feb. 10, 2011.

1 Introduction

Ideally, a microscopic technique does not rely on external labeling, but instead generates contrast with molecular selectivity based on intrinsic molecular features. With respect to selectivity, vibrational techniques potentially have advantages over electronic excitation, since in contrast to generally broad electronic absorptions, even small molecules possess many sharp vibrational resonances. For this reason, adaptations of vibrational spectroscopic techniques for microscopy have recently found a lot of interest, especially in biomedical imaging. Direct infrared (IR) absorption microscopy, however, has severe limitations in spatial resolution due to the long wavelengths employed. Using spontaneous Raman scattering microscopy overcomes this problem, but the low Raman scattering cross sections limit the achievable sensitivity. In addition, the application of spontaneous Raman scattering microscopy is often hampered by the presence of autofluorescence encountered in many samples. This background is often much stronger than the Raman signal.

To circumvent these problems, coherent anti-Stokes Raman scattering (CARS) microscopy has been introduced as a new tool for vibrational microscopy.[1–7] In CARS microscopy, a pump beam at frequency ω_p and a Stokes beam at frequency ω_s are tightly focused onto the sample to generate a CARS signal at frequency $\omega_{as} = 2\omega_p - \omega_s$. A strong resonant CARS signal is generated when the frequency difference $\omega_p - \omega_s$ is tuned to a molecular vibrational resonance with frequency Ω. This provides the chemical selectivity in CARS microscopy.

As such, CARS is a resonance-enhanced four-wave mixing process. Commonly, care has to be taken to fulfill the phase-matching condition $l < l_c = \pi/|\Delta k| = \pi/|k_{as} - (2k_p - k_s)|$, where

k_p, k_s, and k_{as} are wave vectors of the pump, Stokes, and CARS fields, respectively, Δk is the wave vector mismatch, and l_c is the coherence length at which the first maximum of the signal is obtained. However, the phase-matching condition can easily be fulfilled with a collinear beam geometry in CARS microscopy using tight focusing with high numerical aperture objectives.[1] Under this condition, the small interaction lengths l and the large cone angle of the wave vectors of the exciting beams lead to efficient CARS signal generation in the forward direction. At the same time, a strong backward-directed episignal is observed for sample features with sizes on the order of or smaller than the excitation wavelengths.[2] Most of the CARS microscopes developed so far are therefore based on collinear excitation geometry. Objectives with large numerical apertures are employed, and the CARS signal is generated by scanning the tightly cofocused pump and Stokes beams over the sample.[8,9] Scanning systems offer high spatial resolution and axial sectioning capability, but image generation is time consuming. Thus, only very recently has the video-rate regime been reached for strong Raman scatterers.[10]

The latter problem prompted the development of alternative CARS excitation geometries based on wide-field excitation.[11–15] This technique allows for simultaneous imaging of a large field of view. Single-shot imaging capability using nanosecond pulses has been demonstrated, which makes way for investigations of fast biological processes and chemical reactions. Two different approaches of wide-field CARS microscopy have been demonstrated to date. The first employs an excitation geometry involving a dark-field condenser with a high numerical aperture, which generates a "sheet of light" in the sample volume. The wave-matching condition is then satisfied within the light sheet.[12] The second approach, by contrast, uses a nonphase-matching sample illumination scheme. The authors postulated without experi-

Address all correspondence to: Andreas Zumbusch, University of Konstanz, Department of Chemistry, D-78457 Konstanz, Germany. Tel: +49-(0)7531–88 2357; Fax: +49-(0)7531–88 2357; E-mail: andreas.zumbusch@uni-konstanz.de.

mental verification that signal generation here relies on light refraction or scattering within the sample, which eventually brings some portion of the incident radiation into the phase-matching condition. Thus, a CARS signal would only be generated inside the scattering objects and in their immediate vicinity.[14,15] While both approaches are promising, their implementation is technically demanding, since high-power, low-repetition-rate laser systems such as Q-switched Nd:YAG lasers[11–13] or regenerative Ti:sapphire amplifiers[14,15] and special optical elements such as ultradark-field condensers[12] or Cassegrain objectives[15] are necessary. To homogeneously illuminate the sample, both approaches apply homogenizers such as multimode fibers[11–13] or microlens arrays,[15] which inevitably produce speckle noise in the sample plane. Dynamic averaging of the speckle noise by random waggling of the homogenizers will give a smooth image, but also limit the image acquisition speed.[15]

We present a simple video-rate wide-field CARS microscopy experiment using a nonphase-matching wide-field illumination scheme. Picosecond oscillator laser systems are used for excitation. Both pump and Stokes beams are collinearly defocused onto the sample without using any homogenizers, and only excitation light that interacts with scatters can generate a CARS signal. This scheme is a significant simplification of earlier experiments. We demonstrate that signal generation under these focusing conditions indeed relies on scattering within the sample. For this purpose, we systematically investigate the CARS signal generation of polystyrene beads in various refractive index environments and under excitation with different numerical apertures. The chemical selectivity of the method is proven by imaging a mixture of polystyrene and Polymethyl-methacrylate (PMMA) beads using pump and Stokes beams, with frequency differences corresponding to aromatic and aliphatic C-H stretch vibrations. We demonstrate that the system is capable of CARS wide-field imaging at 33 fps and discuss the limitations of this approach.

2 Experiment

2.1 Experiment System

A schematic diagram of the wide-field CARS system is shown in Fig. 1. A Ti: sapphire laser oscillator (Mira HP, Coherent Incorporated, Santa Clara, California) [Full width at half maximum (FWHM) ∼3 ps, repetition rate of 76 MHz] with a tuning range of 700 to 980 nm is used as the pump beam, and an optical parametric oscillator (OPO) (Levante, APE GmbH, Berlin, Germany) (FWHM ∼6 ps, repetition rate of 76 MHz) with a tuning range of 680 to 990 nm is used as the Stokes beam. The experimental setup can be simplified by using the signal output from a 532-nm pumped OPO and residual 1064-nm light of the pump, as pump and Stokes excitation beams, respectively. Pump and Stokes lasers are electronically synchronized (Synchro-lock AP, Coherent Incorporated) and combined in a collinear geometry. To obtain wide-field CARS images, the beams can be focused above or below the sample plane. Defocusing is adjusted by changing the axial position of the focusing objective, which can be either a low NA 10 × objective (HC PL Apo, NA 0.4, Leica, Germany) or a high NA condenser (Pol 0.9 S1, NA 0.9, Leica, Germany), such that an illumination spot with approximately 150 μm diam on the sample is created. To achieve a relatively homogeneous illumination, only the central part of the spot (∼60 μm in diameter) was used to make sure that the variation of the light intensity from the center to the edges of the field of view does not exceed 20%. The CARS signal was detected in forward direction by using a 40× objective (HCX PL Apo, NA 0.85, Leica, Germany). An electron-multiplying charge-coupled device (EMCCD) camera (Andor IXonEM + , Andor Technology PLC, Northern Ireland) is employed to capture the 2-D CARS image. A Nikkor objective (50-mm f/1.8, Nikon, Japan) is used as a tube lens. A short-pass filter (ET680SP-2P8, AHF Analysentechnik AG, Germany) and two band-pass filters (ET Bandpass 605/70-2P and Brightline HC 593/40, AHF Analysentechnik AG, Germany) are put in front of the camera to block the excitation laser beams. The maximum laser powers used in our CARS
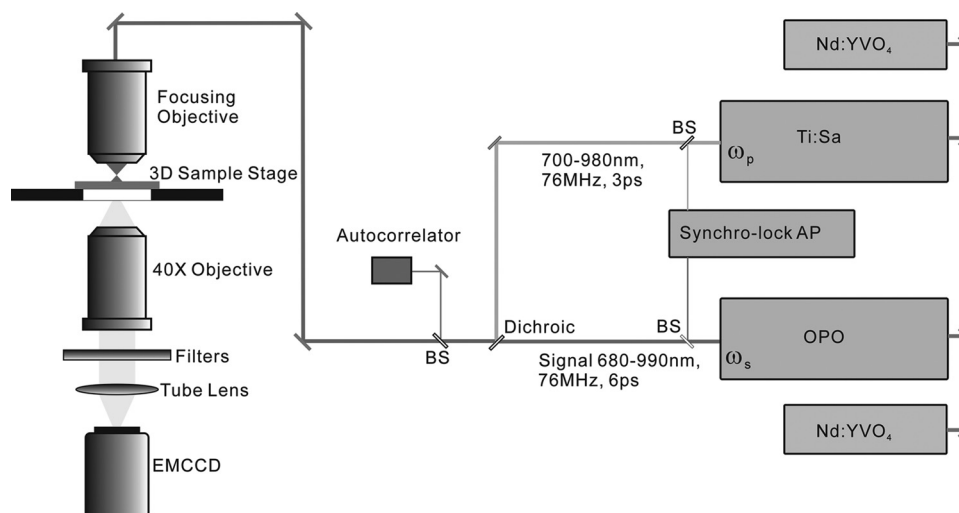

Fig. 1 Experimental layout of the wide-field CARS system. BS is the beam sampler.

experiments are 150 mW for the pump beam and 100 mW for the Stokes beam after the focusing objective. This corresponds to an energy density of 11 μJ/cm^2 (pump) and 7 μJ/cm^2 per pulse. Note that this corresponds to intensities approximately 2000 times lower than those used in a typical raster scanning CARS microscopy experiment. The EMCCD camera allows imaging speeds as high as 33 fps at a resolution of 512×512 pixels.

2.2 Materials

Polystyrene (PS) beads of 6 μm (PPS-6.0, G. Kisker GbR, Germany) as well as PMMA beads of 1 to 10 μm (Polybead PMMA, Polysciences Incorporated, Warrington, Pennsylvania) in diameter are used as samples. The beads are deposited on a 170-μm-thick glass cover slide and immersed in media of different refractive indexes such as air, water, and immersion oil (type F, Leica, Germany).

The *C. elegans* wild-type strain N2 Bristol was used. Embryos were isolated using alkaline hypochlorite solution.[16] To obtain synchronized embryos, adults were washed off nematode growth medium agar plates with M9 buffer. After centrifugation (500 rpm) for one minute, pelleted worms were washed with M9 buffer until the supernatant was clear of bacteria. The worm pellet was lysed by using an alkaline hypochlorite solution (bleaching), which was composed of 0.3-ml NaOH, 0.6-ml 12% Na-hypochlorite, and 4.1-ml H_2O. After bleaching for two minutes, the lysis reaction was stopped by diluting with M9 buffer. The eggs were pelleted and washed several times with M9 buffer. After the last wash, the eggs were suspended in 1-ml M9 buffer.

3 Results and Discussion

To demonstrate that the signal generated by this simple wide-field illumination scheme is CARS, we imaged mixtures of PS beads (6 μm diam) and PMMA beads (1 to 10 μm diam) deposited on 170-μm-thick cover slides as samples (Fig. 2). The CARS nature of the detected signal is proven by changing the time delay between pump and Stokes pulses. As expected, the signal disappears completely when the two beams are not temporally overlapped. To show that the signal is not merely due to the generation of nonresonant CARS, but indeed carries information about the chemical nature of the sample, images of a mixture of PS and PMMA beads were recorded. Since PS con-
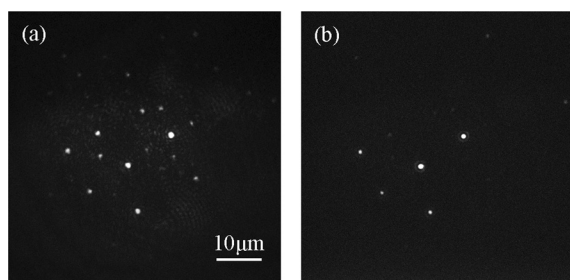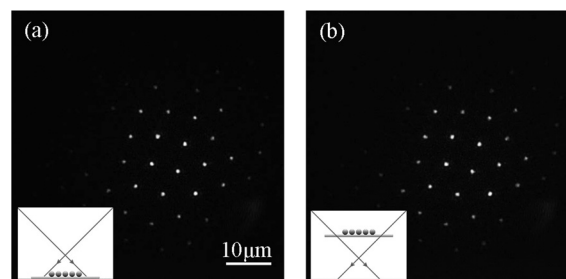

Fig. 3 Comparison of CARS images of 6-μm PS beads with different defocusing geometries. (a) Focusing above the sample, and (b) focusing below the sample. The Raman shift is 3050 cm^{-1}. The exposure time is 0.1 s.

tains both aromatic and aliphatic CH, whereas PMMA contains only aliphatic CH, the first image was recorded at 2940 cm^{-1}, the maximum of the CH$_3$-stretch vibration in PMMA, whereas the second image was recorded at 3050 cm^{-1}, the aromatic CH-stretch resonance of PS. As expected, Fig. 2 shows that both types of beads can be distinguished in the CARS images.

To shed light on the phase-matching mechanism necessary for efficient CARS signal generation, we performed two types of experiments. In the first, we used different numerical apertures to illuminate the sample. Both a low NA objective (10×, NA 0.4) and a high NA condenser (NA 0.9) were employed. Under the condition that direct phase-matching is necessary for signal generation, this would lead to different signal intensities. Instead, within the experimental errors, the same CARS intensities are observed, which is in contrast to earlier wide-field CARS microscopy experiments.[11–15] This supports the notion that CARS signal generation in this collinear illumination approach in a nonphase-matching geometry mainly stems from laser refraction and scattering in the sample. It is noteworthy that when we changed the position of the common focus of the pump and Stokes beam from above the sample, to below the sample also no change in signal intensity was observed (Fig. 3). Excitation beams could be focused 200 μm above or below the sample plane. Here, care has to be taken not to focus too close to the sample plane. Otherwise, the strong CARS signal from the surrounding medium generated in the focus will dominate the wide-field image.

The second experimental proof that our CARS signal comes from light refraction or scattering is the dependence of signal generation on the refractive medium surrounding the resonant features in the sample. Increasing the refraction of the laser beams inside the sample should lead to a concomitant rise of the CARS signal. To simulate these conditions, PS beads ($n_{polystyrene}$ = 1.55) were immersed in media of various refractive indices (air, n_{air} = 1; water, n_{water} = 1.33; or index-matching oil, n_{oil} = n_{glass} = 1.52). The intensity profile of CARS images with PS beads in these refractive index environments are compared in Fig. 4. The imaging conditions are the same. It is obvious that the contrast of the images significantly increased for higher differences of refractive index between the PS beads and the surrounding medium. The signal-to-background ratio for PS beads in oil is 3:1, in water 6:1, and in air 10:1. In no case was any noticeable background detected due to nonresonant CARS signal generation. This is in stark contrast to normal raster scanning CARS microscopy experiments, where this is commonly only

Fig. 2 CARS images of mixtures of PS beads of 6 μm as well as of PMMA beads 1 to 10 μm in diameter. The Raman shift is (a) 2940 cm^{-1} (aliphatic CH$_3$-stretch) and (b) 3050 cm^{-1} (aromatic CH-stretch). The exposure time is 0.2 s. As expected, the PMMA beads are only visible with excitation in the aliphatic CH-region.
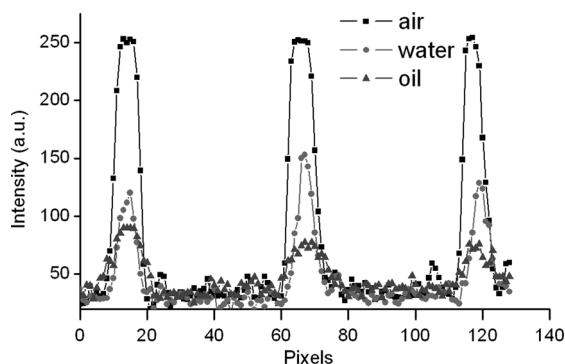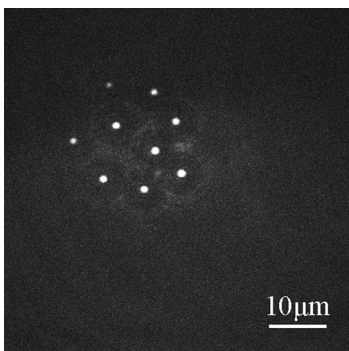
Fig. 4 Intensity profile of PS beads immersed in air, water, and oil. The Raman shift is 3050 cm^{-1} and the exposure time is 0.1 s. The decreased contrast is due to reduced refraction of the excitation light.
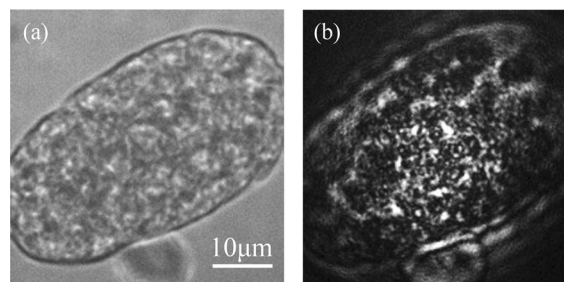

Fig. 5 Images of isolated *C. elegans* embryos. (a) Bright field image and (b) CARS image taken at the aliphatic CH_2 resonance at 2850 cm^{-1}. The exposure time is 0.5 s.

true if resonant features are surrounded by air. Based on the experiments described, we conclude that refraction and scattering of the excitation laser in the sample lead to appreciable phase matching and thus to efficient CARS signal generation, even under a nonphase-matching collinear excitation geometry. For particle sizes of the samples investigated here, refraction effects are dominant. However, for smaller features, scattering can also contribute to the phase-matching.

Based on this easy-to-implement wide-field CARS microscope, one can generate video-rate CARS images, as highlighted in Video 1. A sample with PS beads in water is moved. An EMCCD camera is used to get the video, and 33-fps imaging speed is demonstrated. The setup also suits itself to record CARS images of living samples. As an example, we used the wide-field CARS microscope to image embryos of *C. elegans in vitro*. Figure 5(a) is the bright field image and Fig. 5(b) is the CARS image taken at the 2850 cm^{-1} CH_2-symmetric stretch vibration of lipids.

While high frame rates can be achieved with this type of experiment, its disadvantages should not go unmentioned. First of all, the excitation scheme relies on refractive index changes and scattering within the sample. Thus, interesting applications such as the monitoring of chemical reactions in flow cells[17] cannot be tackled like this, even if the fast imaging capability would be of interest here. Second, our approach does not lend

itself to investigations requiring 3-D spatial resolution, since the depth resolution will be worse than 10 μm. It is ultimately limited by the depth of focus of the collecting lens. While this approach is simple, this is a severe disadvantage compared to wide-field CARS microscopy using phase-matched illumination.[11–13] However, due to its simplicity and fast imaging capability, non-phase matched CARS microscopy can still be a useful tool, for example, in cytometric applications.[18]

4 Conclusions

We present an approach to implementing a video-rate wide-field CARS microscopy experiment based on collinear non-phasematching sample illumination geometry. It is demonstrated that refraction of excitation light leads to efficient CARS signal generation. While the setup has shortcomings such as the lack of 3-D resolution and the need for heterogeneous samples, our system has advantages over conventional wide-field CARS, including simple implementation, very low excitation powers, and high imaging speed. Examples of CARS micrographs of polystyrene and PMMA beads as well as of embryos of *C. elegans* are given, and the chemical selectivity of our system is demonstrated.

Video 1 Movie of a sample with 6-μm PS beads in water, which was moved by hand. The Raman shift is 3050 cm^{-1} and the exposure time is 0.03 s. (Quick Time, 2.4 MB).
[URL: http://dx.doi.org/10.1117/1.3533707]

References

1. A. Zumbusch, G. R. Holtom, and X. S. Xie, "Three-dimensional vibrational imaging by coherent anti-Stokes Raman scattering," *Phys. Rev. Lett.* **82**(20), 4142–4145 (1999).
2. A. Volkmer, J. X. Cheng, and X. S. Xie, "Vibrational imaging with high sensitivity via epidetected coherent anti-Stokes Raman scattering microscopy," *Phys. Rev. Lett.* **87**(2), 023901 (2001).
3. J. X. Cheng, L. D. Book, and X. S. Xie, "Polarization coherent anti-Stokes Raman scattering microscopy," *Opt. Lett.* **26**(17), 1341–1343 (2001).
4. J. X. Cheng, A. Volkmer, L. D. Book, and X. S. Xie, "Multiplex coherent anti-Stokes Raman scattering microspectroscopy and study of lipid vesicles," *J. Phys. Chem. B* **106**(34), 8493–8498 (2002).

5. A. Volkmer, L. D. Book, and X. S. Xie, "Time-resolved coherent anti-Stokes Raman scattering microscopy: imaging based on Raman free induction decay," *Appl. Phys. Lett.* **80**(9), 1505–1507 (2002).

6. E. O. Potma, C. L. Evans, and X. S. Xie, "Heterodyne coherent anti-Stokes Raman scattering (CARS) imaging," *Opt. Lett.* **31**(2), 241–243 (2006).

7. F. Ganikhanov, C. L. Evans, B. G. Saar, and X. S. Xie, "High-sensitivity vibrational imaging with frequency modulation Coherent anti-Stokes Raman scattering (fm CARS) microscopy," *Opt. Lett.* **31**(12), 1872–1874 (2006).

8. J. X. Cheng and X. S. Xie, "Coherent anti-Stokes Raman scattering microscopy: instrumentation, theory, and applications," *J. Phys. Chem. B* **108**(3), 827–840 (2004).

9. M. Müller and A. Zumbusch, "Coherent anti-Stokes Raman scattering (CARS) microscopy," *Chem. Phys. Chem.* **8**(15), 2156–2170 (2007).

10. C. L. Evans, E. O. Potma, M. Puoris'haag, D. Cote, C. P. Lin, and X. S. Xie, "Chemical imaging of tissue in vivo with video-rate Coherent anti-Stokes Raman Scattering microscopy," *Proc. Natl. Acad. Sci. USA* **102**(46), 16807–16812 (2005).

11. C. Heinrich, S. Bernet, and M. Ritsch-Marte, "Wide-field coherent anti-Stokes Raman scattering microscopy," *Appl. Phys. Lett.* **84**(5), 816–818 (2004).

12. C. Heinrich, A. Hofer, A. Ritsch, C. Ciardi, S. Bernet, and M. Ritsch-Marte, "Selective imaging of saturated and unsaturated lipids by wide-field CARS-microscopy," *Opt. Express* **16**(4), 2699–2708 (2008).

13. C. Heinrich, A. Hofer, S. Bernet, and M. Ritsch-Marte, "Coherent anti-Stokes Raman scattering microscopy with dynamic speckle illumination," *New J. Phys.* **10**(2), 023029 (2008).

14. I. Toytman, K. Cohn, T. Smith, D. Simanovskii, and D. Palanker, "Wide-field coherent anti-Stokes Raman scattering microscopy with non-phase-matching illumination," *Opt. Lett.* **32**(13), 1941–1943 (2007).

15. I. Toytman, D. Simanovskii, and D. Palanker, "On illumination schemes for wide-field CARS microscopy," *Opt. Express* **17**(9), 7339–7347 (2009).

16. H. F. Epstein, D. L. Casey, and I. Ortiz, "Myosin and paramyosin of caenorhabdities elegans embryos assemble into nascent structures distinct from thick filaments and multi-filament assemblages," *J. Cell Biol.* **122** (4), 845–858 (1993).

17. D. Schafer, J. A. Squier, J. van Maarseveen, D. Bonn, M. Bonn, and M. Müller, "In situ quantitative measurement of concentration profiles in a microreactor with submicron resolution using multiplex CARS microscopy," *J. Am. Chem. Soc.* **130**(35), 11592–11593 (2008).

18. H. W. Wang, N. Bao, T. T. Le, C. Lu, and J. X. Cheng, "Microfluidic CARS cytometry," *Opt. Express* **16**(8), 5782–5789 (2008).